Australian Earthquake Engineering Society 2019 Conference, Nov 29- Dec 1,
Newcastle City Hall, New South Wales

The application of mixed-mode de-cohesion criteria in masonry finite element analysis

Nie, Y[1], Sheikh, A.[1,2], Griffith, M.[1,2], Visintin, P.[1,2] and Vaculik, J.[1,2]

1. School of Civil, Environmental and Mining Engineering, University of Adelaide, Australia.
2. Bushfire and Natural Hazards Cooperation Research Centre, Australia.

Abstract: This paper introduces a novel finite element modelling approach for masonry structures. The mixed-mode de-cohesion criteria is applied on a detailed and a simplified finite element model separately to predict the behaviour of masonry walls under different loading conditions, including the in-plane load and the out-of-plane load. The joint in the detailed model is composited by interfaces and mortar layer, whilst in the simplified model it is represented by a pair of interfaces. The interfacial constitutive model includes damage initiation and damage involution that can simulate the post-failure behaviour of masonry joints under tensile, shear, compressive and their combined loads. The failure of masonry structure under high compression can be represented by brick failure with concrete damage plasticity criteria. Performance of the detailed modelling approach is evaluated by comparing modelling results with experimental results.

Keywords: masonry structures, finite element model, cohesive model

1. Introduction

The application of finite element model (FEM) in analysing masonry structures has been widely acceptable, especially for some historical buildings that are not allowed to conduct destructive tests. The failure of unreinforced masonry wall (URM) includes both interaction de-bonding and brick material damage, thus it is necessary to make use of proper interaction criteria and material criteria simulating the behaviour of masonry wall.

Common used simulation strategies of masonry walls are: 1) detailed micro-modelling strategy; 2) simplified micro-modelling strategy as well as 3) macro-modelling strategy (Lourenco, 1997). The detailed model is most close to real masonry structure geometry but its running cost is relatively high, and sometimes only explicit algorithm can overcome the convergence difficulties (Andreotti et.al, 2018). In contract, the macro-model without mortar joints has highest computation efficiency but it has to scarify accuracy to some extent (Lofti & Shing, 1991; Anthoine, 1995). A compromised method is using simplified micro-model that simplifies mortar joints as a non-thickness interface, which is also the most popular modelling approach (Lourenco & Rots, 1997; Lofti & Shing, 1994; Abdulla et.al 2017).

A masonry structure is extremely sensitive to seismic force, so it is common that masonry buildings collapsing occur in earthquake disasters. A seismic load has two horizontal waves that are perpendicular to and parallel to masonry walls respectively, resulting in in-plane loads and out-of-plane loads on structures. As shown in Figure 1, the whole wall in the building fall down due to the seismic load being perpendicular to the wall surface as shown in Figure 1 (a), whereas the lateral wall under a parallel seismic load has inclined cracks as shown in Figure 1(b).

This paper evaluates the performance of masonry walls under in-plane loads and out-of-plane loads by applying a de-cohesive mixed constitutive model in expended brick-brick interface (simplified model) and mortar-brick interface (detailed model). The interaction constitutive model is proposed by Camanho & Davila (2002) to simulate the delamination of composite material. A more detailed discussion of interaction behaviour is presented in the next section.

(a) wall collapse under out-of-plane load (b) wall failure under in-plane load

Figure 1 Building collapse under seismic loads (Gautam et.al 2016)

2. Interaction Behaviour

Pluijm (1992) investigated the tensile and shear behaviours of masonry by a series of tests and summarized their behaviours as shown in Figure 2. In the pre-failure stage, both the normal and shear behaviour of masonry joints are elastic, so elastic modulus or elastic stiffness can describe the traction-separation relationship. In the post-failure stage, the stress-displacement curve has a non-linear softening relation which can be expressed by exponential equations (Nazir, 2014) or a damage model (D'Altri, 2018). This paper adopts damage mechanism to describe the post-failure behaviour of masonry joints.

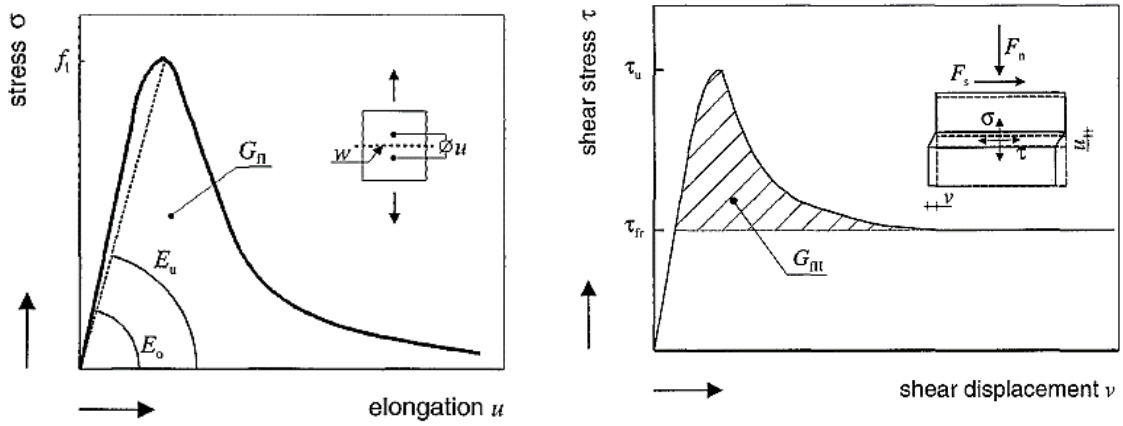

(a) normal tensile behaviour (b) shear behaviour

Figure 2 Masonry joint behaviour in normal and shear direction (Pluijm, 1992)

The connections between brick-brick or brick-mortar are simulated by zero-thickness de-cohesion element as shown in Figure 3. The de-cohesive element comprises of 8 nodes and its constitutive behaviour is described by the relation between separations (displacements) and tractions (stresses) across the interface.

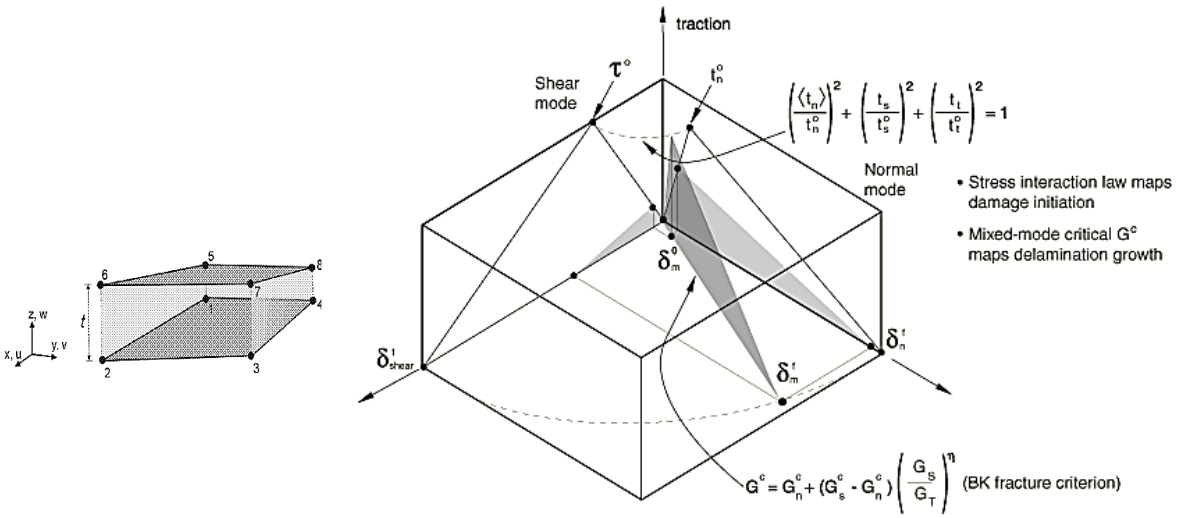

Figure 3 De-cohesive element and its mix-mode response (Abaqus Users' Manual, 2014)

The linear elastic traction-separation behaviour is expressed by an uncoupled equation:

$$\begin{bmatrix} t_n \\ t_s \\ t_t \end{bmatrix} = \begin{bmatrix} K_{nn} & 0 & 0 \\ 0 & K_{ss} & 0 \\ 0 & 0 & K_{tt} \end{bmatrix} \begin{bmatrix} u_n \\ u_s \\ u_t \end{bmatrix} \tag{1}$$

where: t_n, t_s and t_t are the traction stress in tensile, shear I and shear II directions; K_{nn}, K_{ss} and K_{tt} are the elastic stiffness in the tensile, shear I and shear II directions; u_n, u_s and u_t are the separation displacement in in tensile, shear I and shear II directions.

The initiation of damage degradation of interaction can be activated by either maximum stress criterion or quadratic stress criteria. In this paper, the maximum stress criterion is applied in the detailed model while quadratic stress criteria is applied in the simplified model:

$$\max\left\{\frac{\langle t_n \rangle}{f_n}, \frac{t_s}{f_s}, \frac{t_t}{f_t}\right\} = 1 \tag{2.a}$$

$$\left(\frac{\langle t_n \rangle}{f_n}\right)^2 + \left(\frac{t_s}{f_s}\right)^2 + \left(\frac{t_t}{f_t}\right)^2 = 1 \tag{2.b}$$

Where: f_n, f_s and f_t are the maximum stress in tensile, shear I and shear II directions measured by direct tensile test and direct shear test, as the peak values shown in Figure 2. Macaulay bracket function $\langle t_n \rangle = (|t_n| + t_n)/2$.

The damage evolution process is controlled by the damage variable *D* and the predicted contact stress $(\bar{t}_n, \bar{t}_s, \bar{t}_t)$ calculated by elastic stiffness:

$$t_n = (1-D)\bar{t}_n, \qquad t_s = (1-D)\bar{t}_s, \qquad t_t = (1-D)\bar{t}_t \tag{3}$$

The damage variable *D* is calculated by a linear softening equation:

$$D = \frac{u_m^f(u_m^{max} - u_m^0)}{u_m^{max}(u_m^f - u_m^0)} \tag{4}$$

Where: u_m^f, u_m^{max} and u_m^0 are the total failure displacement, maximum effective displacement and initial damage displacement respectively, as shown in Figure 4.

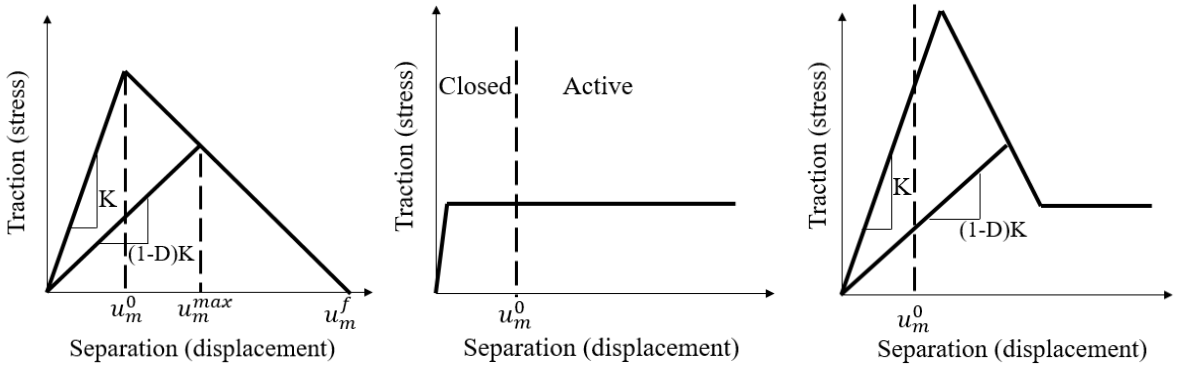

(a) traction-separation behaviour

(b) penalty friction behaviour

(c) combined behaviour with traction-separation law and penalty friction behaviour

Figure 4 Combined interaction constitutive model

In the damage evolution process the total failure displacement u_m^f is calculated by the mixed fracture energy G_{mixed}^C:

$$u_m^f = 2G_{mixed}^C / f_{eff} \tag{5}$$

Where: f_{eff} is the effective traction stress at damage initiation which is combined by shear mode and normal mode traction stresses. G_{mixed}^C is the mixed energy obtained Benzeggagh-Kenane (B-K) fracture criterion (Benzeggagh & Kenane, 1996):

$$G_{mixed}^C = G_n^f + (G_s^f - G_n^f)\left(\frac{G_s + G_t}{G_s + G_t + G_n}\right)^m \tag{6}$$

Where: G_n^f and G_s^f are the fracture energy determined from direct tensile test and direct shear test respectively; G_n, G_s and G_t are the effective energy in the tensile, shear I and shear II direction respectively. m is the cohesive property parameter for the material, the author recommends m =2 for masonry joints here.

It is common that implicit constitutive model with softening and damage degradation behaviour has convergence problems. To overcome the potential convergence difficulties, a viscosity coefficient, μ, is adopted for the stabilization of the FE model. The value of μ is recommend as 0.002 based on Abdulla's (2017) parametric study for masonry finite element models. Surface based cohesive behaviour is applied in this project to simulate the brick-brick interface (simplified micro-model) or brick-mortar interface (detailed micro-model). Compared with element based cohesive behaviour, surface based behaviour has an advantage that it allows the

combination of traction-separation behaviour (Figure 4a) with compressive-fractional behaviour (Figure 4b). If the masonry specimen is under compressive and shear loading simultaneously, the interface has the composited behaviour in shear direction as shown in Figure 4(c). For the shear behaviour, if the traction-separation is undamaged, the cohesive is active but penalty friction is closed. Once the traction-separation start damaging, the penalty becomes active and contributes to the shear stress, so the shear stress is the combination of traction-separation and penalty friction.

3. Finite Element Model

3.1 Small scale masonry couplet specimen

To verify the reliability of the interaction model introduced above, a small scale masonry FE model coupled by two bricks and a mortar layer is built for comparing its modelling results with experimental results under pure tensile load and combined shear-compressive load, as shown in Figure 5. Table 1 lists all input data used for FE model of the small scale masonry couplet FE model.

Table 1 Damage parameters for nonlinear couplet models

	Normal strength f_t (N/mm^2)	Cohesive parameter c (N/mm^2)	Friction coefficient μ	Shear strength f_s (N/mm^2)	Tensile fracture energy (Nmm/mm^2)	Shear fracture energy (Nmm/mm^2)
Tension	0.28	0.3	0	0.3		0.188
Shear -0.1MPa pressure		0.87	0.75	0.945		0.071
Shear -0.5MPa pressure	0.3	0.87	0.75	1.245	0.012	0.123
Shear -1.0MPa pressure		1.2	1	2.2		0.188

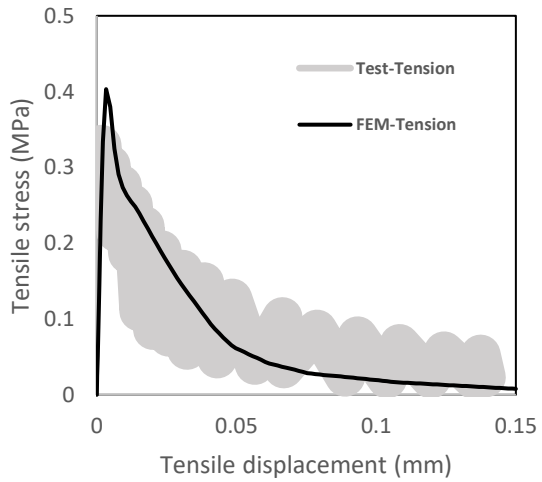

(a) Tensile stress-displacement

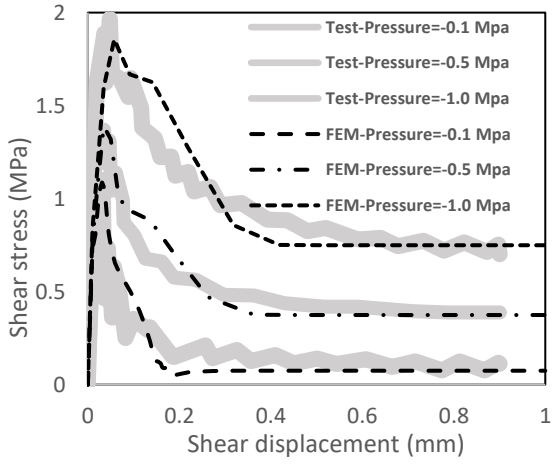

(b) Shear stress-displacement

Figure 5 Comparison of the damage behaviours of a masonry couplet obtained from experimental testing (Pluijm 1999) and FE modelling

The material properties of brick is elastic and the linear elastic stiffness of interaction is defined based on the modelling strategies. For detailed micro-model, the contact elastic stiffness is equal to 500 times the stiffness of the under-laying elements (D'Altri, 2018), while for the simplified micro-model, the contact elastic stiffness is defined as:

$$K_{nn} = \frac{E_b\, E_j}{h_j\,(E_b\, -\, E_j)}, \qquad K_{tt} = K_{ss} = \frac{G_b\, G_j}{h_j\,(G_b\, -\, G_j)} \tag{7}$$

Where: E_b and E_j are the Elastic modulus of brick and mortar joint respectively; G_b and G_j are the shear modulus of brick and mortar joint respectively; h_j is the height of the mortar joints.

3.2 Detailed Micro-Model (In plane load)

A finite element model for the masonry under pre-compression and in-plane shear load is built as shown in Figure 6. The FE model technique proposed by D'Altri et.al (2018) used "texture units", a composite unit including both brick and mortar, to assembly masonry wall, which reduces the number of interfaces and improves the computing efficiency. The nonlinear behaviour of both brick and mortar are simulated by concrete damage plasticity (CDP) constitutive model (Lee & Fenves, 1998). Table 2 and Table 3 list all input data for the detailed micro FE model for masonry wall under in-plane load. The modelling results are compared with experiments conducted by Vermeltfoort and Raijmakers (1993). Figure 7 shows the failure pattern of FE models. Comparison between modelling results and experimental results is shown in Figure 8.

Table 2 Interface properties of the in-plane wall model

	Tensile strength f_t (N/mm^2)	Shear strength f_s (N/mm^2)	Tensile fracture energy G_I^f (Nmm/mm^2)	Shear fracture energy G_{II}^f (Nmm/mm^2)
Pressure= -0.3	0.1	0.3	0.01	0.2
Pressure= -1.21	0.12	0.2	0.012	0.1
Pressure= -2.12	0.1	0.2	0.01	0.1

Table 3 Non-linear properties of bricks and mortar for CDP model of in-plane wall

Mortar				Brick			
Elastic modulus (MPa) 850; 1200		Poisson's ratio 0.15		Elastic modulus (MPa) 16700		Poisson's ratio 0.15	
Tensile nonlinear uniaxial behaviour		Compressive nonlinear uniaxial behaviour		Tensile nonlinear uniaxial behaviour		Compressive nonlinear uniaxial behaviour	
Stress (MPa)	Inelastic strain	Stress (MPa)	Inelastic strain	Stress (MPa)	Inelastic strain	Stress (MPa)	Inelastic strain
1.5	0	7	0	3.5	0	9	0
0.1	0.002	7.5	0.002	0.3	0.002	9.5	0.001
		0.4	0.015			0.6	0.007

(FE model of masonry walls under 0.3MPa and 2.12MPa pre-pressure have 850 MPa Elastic modulus mortar, while FE model of masonry wall under 1.21MPa pre-pressure has 1200 MPa Elastic modulus mortar.)

Figure 6(a) shows the in-plane wall finite element model geometry and different textured units distribution, and Figure 6(b) shows the loading conditions for the experimental specimen and

its general failure patterns. There totally four masonry wall specimens were tested, two walls under 0.3 MPa vertical pre-pressure, one wall under 1.21 MPa vertical pre-pressure and one wall under 2.12MPa pre-pressure. Both experimental results and modelling results found a diagonal crack as the failure patterns for in-plane wall specimens. Firstly, there were short horizontal cracks appear on the top and bottom corners, and then tensile and shear failure happens on some head and bed joints. Finally, a continuum diagonal crack presented in the wall. In Figure 7(a), minimum principle stress contour can help predict the next cracks happening position where negative stress concentrated due to the reason that interface tensile stress reduced. Similar to the experimental results, horizontal cracks found in corners initially, and then diagonal cracks appeared in the wall centre. In Figure 7(b), Concrete damage plasticity (CDP) model predicted the location of brick cracks occurs as well as the compressive crushing failure.it can be seen that the most critical compressive crushing exists on the corners.

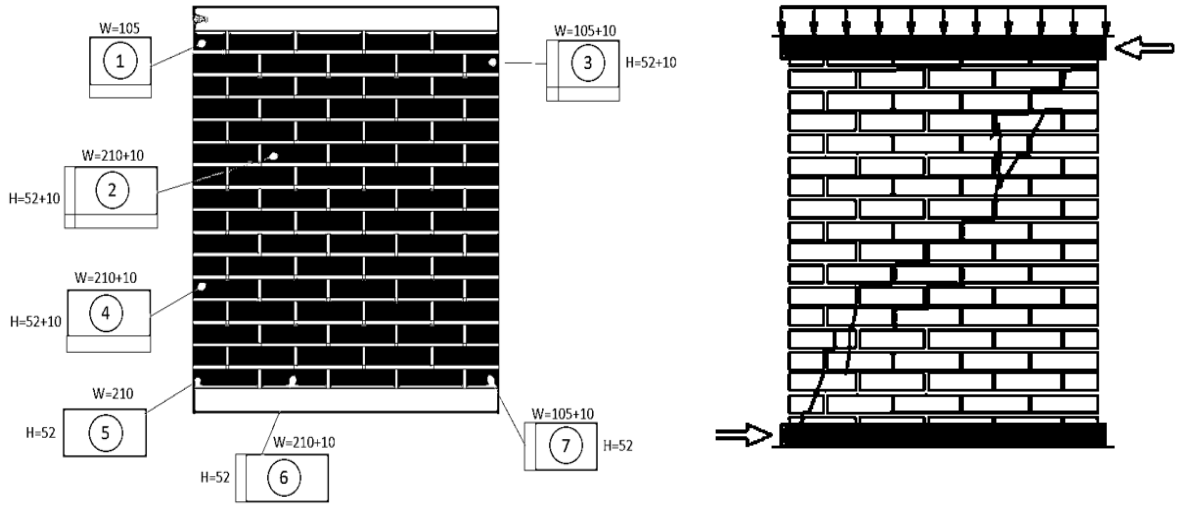

(a) finite element model assembly (b) experiment specimen with cracking pattern

Figure 6 In-plane masonry wall geometry

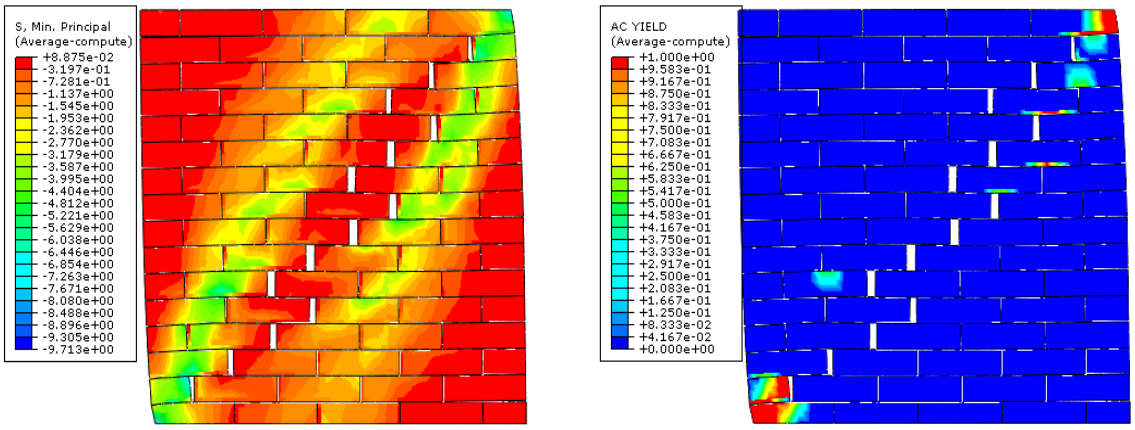

(a) Minimum principle stress contour (b) brick yield patterns

Figure 7 Failure patterns of modelling walls (10 times scale deformation) for specimens under 0.3MPa pre-pressure

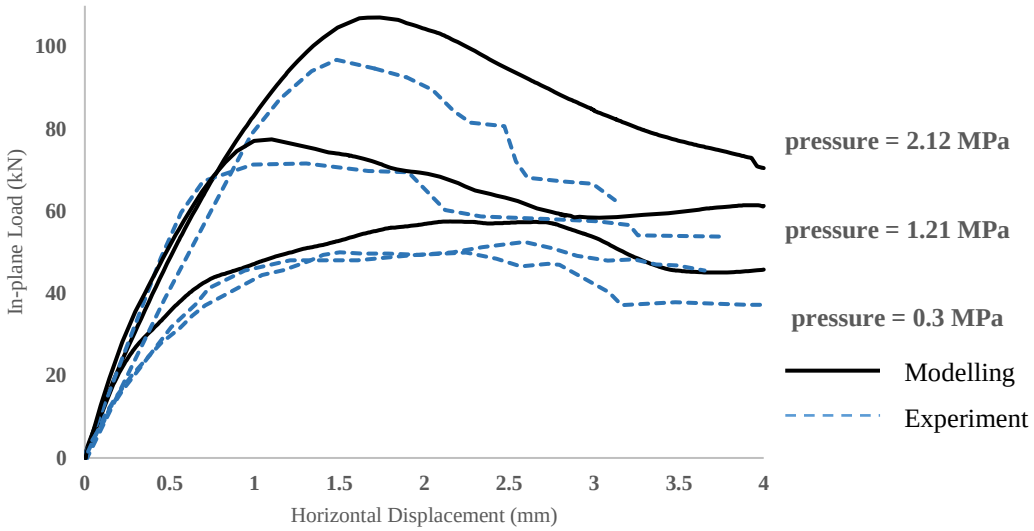

Figure 8 Load-displacement relation of in-plane wall testing

In the Figure 8, finite element models can predict the pre-failure and post-failure behaviour of masonry walls under in-plane shear loads effectively, but modelling results relatively overestimate the peak load of each wall. For walls under low pre-pressure (0.3 MPa), their non-linear behaviour includes a hardening part and a long consistent load plateau, while the plateau will decrease finally with the displacement increment. For walls under high pre-pressure (1.21 MPa and 2.12 MPa), their non-linear behaviour includes a short hardening and a followed long softening. It can be seen for the curves in Figure 8 that, the difference of final post-failure loads is relatively smaller than the difference of peak loads. The reason is that peak load is supported by shear and tensile capacity of joints, so different pre-pressures will result in different shear frictional capacities. However, with the increment of displacement, joint failure happened and lose their cohesive capacity, the failure load of masonry structures will be determined by wall's overturning capacity, namely, the compressive capability of bricks in corners.

3.3 Simplified Micro-Model (Out-of-plane load)

To estimate the performance of masonry wall under out-of-plane pressure load, two FE models with different configurations are simulated. One model is created based on single leaf masonry panel tested by Ng (1996) with 1190 mm height, 795 mm width and 53 mm thickness, so the height-width (H/W) ratio is about 1.5, as shown in Figure 9. Another model is created for the clay brick wall (Griffith's & Vaculik, 2007) with 2500 mm height, 4000 mm width and 110 mm thickness, so the height-width (H/W) ratio is around 0.63, as shown in Figure 9. Table 4 lists the input interfacial properties used for FE models of two type out-of-plane walls. Table 5 presents input data for FE model based on CDP material model of Ng' (1996) single leaf panel and Table 6 lists input data for FE model using Drucker-Prager material model of the clay brick wall test by Griffith's & Vaculik's (2007).

Since the sizes of out-of-plane walls are much larger than in-plane walls sizes, the simplified micro-modelling strategy is more suitable for the simulation of out-of-plane wall. Besides, a quasi-static implicit dynamic analysis procedure is used to accelerate analysis time and save data storage. The analysis needs inertia parameters, such as density of the masonry wall, to solve motion equations.

Table 4 Interface properties of the out-of-plane wall model

	Tensile strength f_t (N/mm^2)	Shear strength f_s (N/mm^2)	Tensile fracture energy G_I^f (Nmm/mm^2)	Shear fracture energy G_{II}^f (Nmm/mm^2)
H/W=1.5	0.24	0.44	0.01	0.022
H/W=0.63	0.09	0.13	0.009	0.03

Table 5 Properties of expended bricks for CDP model (out of plane with 1.5 H/W ratio)

Elastic modulus (MPa)		Poisson's ratio		Density kg/m^3	
16700		0.15		2500	
Tensile nonlinear uniaxial behaviour		Compressive nonlinear uniaxial behaviour		Dilation angle	10
Stress (MPa)	Inelastic strain	Stress (MPa)	Inelastic strain	Eccentricity	0.1
3.5	0	11	0	f_{b0}/f_{c0}	1.16
0.3	0.002	11.5	0.001	K	0.667
		0.6	0.007	Viscosity parameter	0.002

Table 6 Properties of expended bricks for DP model (out of plane with 0.63 H/W ratio)

Elastic modulus (MPa)	Poisson's ratio	Angle of friction	Flow Stress Ratio	Dilation angle
3540	0.15	36	1	11.3

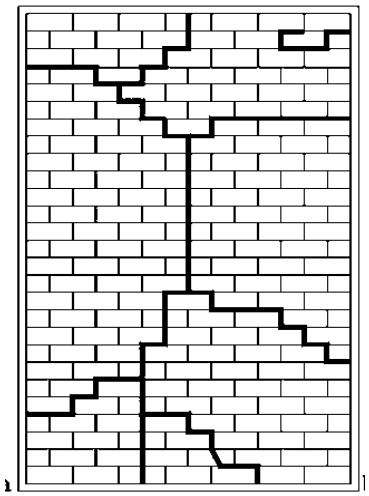

(a) H/W = 1.5 (left, Ng 1996)

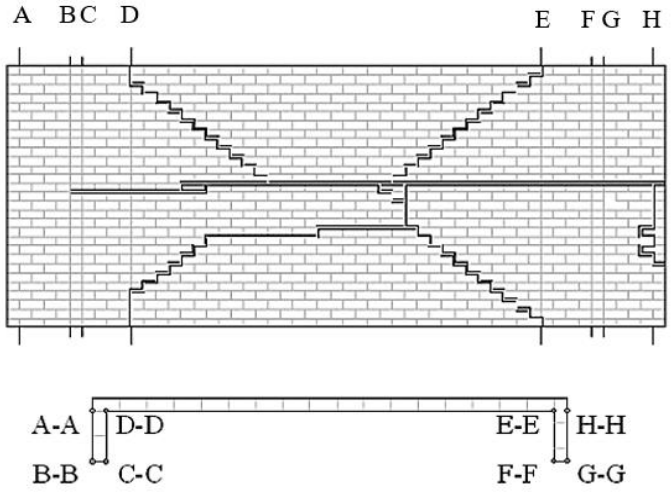

(b) H/W = 0.63 (right, Griffith & Vaculik 2007)

Figure 9 Masonry wall with different geometry

Experimental result provided maximum load capacity and load-pressure relation from 0 to 0.5mm displacement. The FE model estimates the load-pressure relation over 50mm, and it predicts a softening process for the masonry wall, as shown in Figure 10. The cracking pattern and stress contour of FE model are shown in Figure 11.

Figure 10(a) compares the modelling results with experimental results as well as D'Altri et.al (2018) modelling results. The experimental results did not capture the post-failure behaviour of the masonry wall but it provided the peak load which can be predicted by the FE model. Difference with the modelling result from D'Altri et.al (2018) which shows the masonry will be collapsed suddenly after the peak load, the FE model proposed by this paper predicts the masonry wall has much longer post-failure behaviour with a gradually softening curve, as shown in Figure 10(b). Maximum principle stress contour and cracking patterns are shown in Figure 11(a) and Figure 11(b) respectively. The cracking pattern includes four diagonal cracks caused by two-way bending moment and one vertical crack caused by horizontal bending moment. The air-bag pressure firstly resulted in the two-way bending deformation and then the four diagonal crack happened, which is followed by a vertical crack caused by horizontal bending moment. The maximum principal stress contour shows that four corners experienced the most critical damage. In contrast, other positions have relatively lower stress concentration.

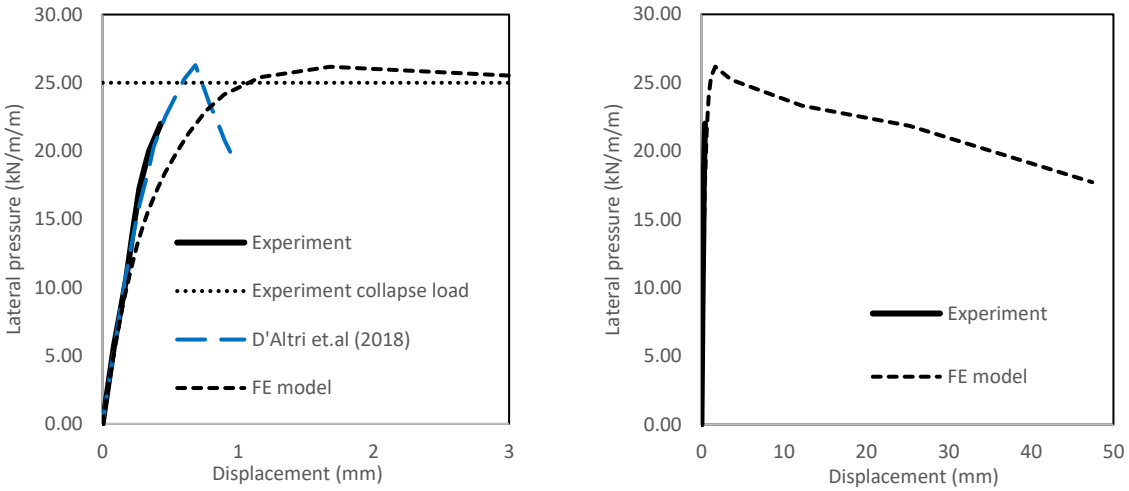

(a) displacement range 0-3mm (b) displacement range 0-50mm

Figure 10 Load-displacement relation for H/W=1.5 masonry wall

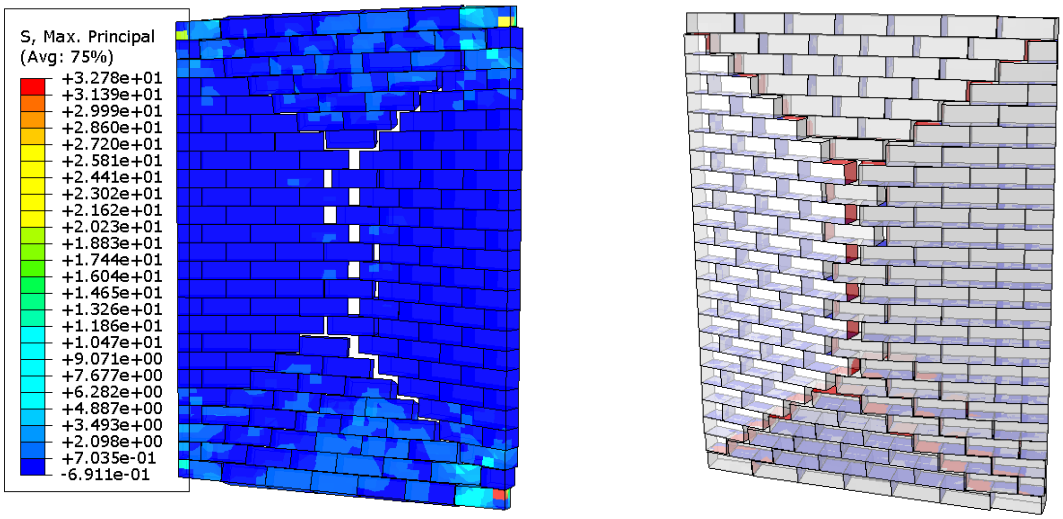

(a) Maximum stress contour (back side) (b) cracking pattern (front side)

Figure 11 Failure patterns of H/W = 1.5 wall FE models

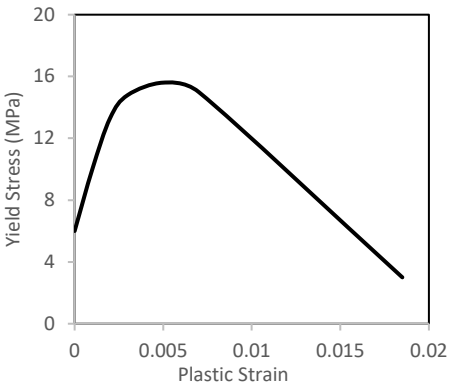

(a) Hardening behaviour of a brick under uniaxial compression obtained from analytical model

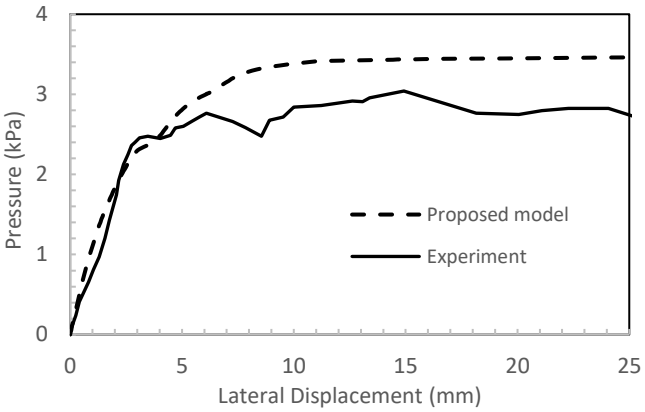

(b) Pressure – lateral displacement relation for a masonry wall (H/W = 0.63)

Figure 12 Material behaviour and structure response:

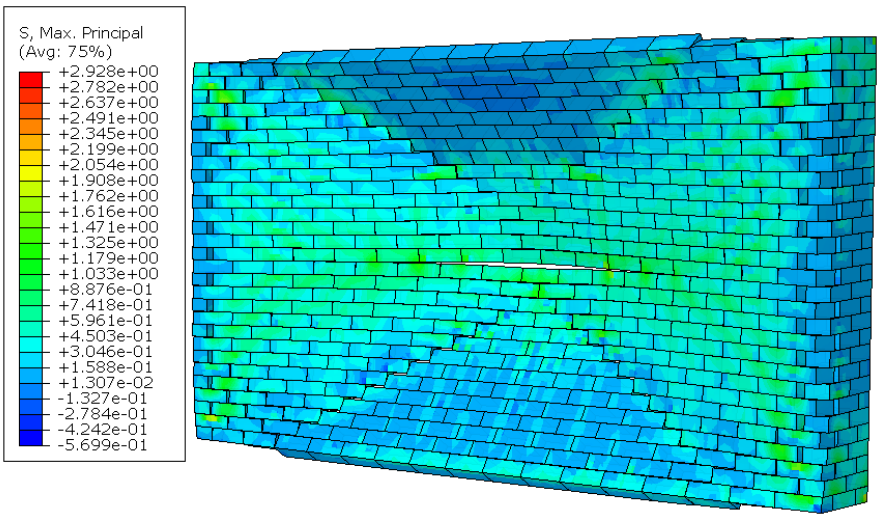

(a) Maximum stress contour (back side)

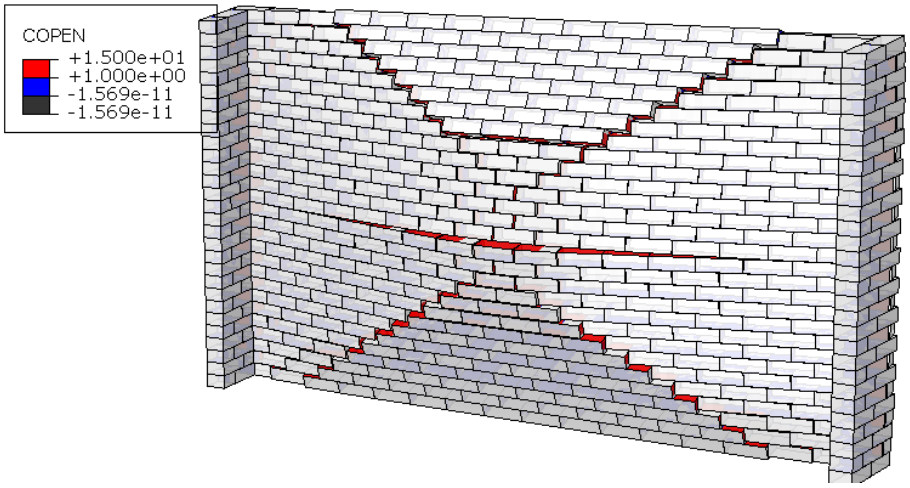

(b) cracking pattern (front side)

Figure 13 Failure patterns of H/W = 0.63 wall FE models (10 times scale)

Difference with the H/W=1.5 wall FE model, the nonlinear material constitutive model for simulating H/W=0.63 wall FE model is Drucker-Prager (DP) plasticity model. The material parameters are summarized in the Table 6, and the hardening behaviour of expended brick is obtained based on Kaushik et.al (2007) analytical model as shown in Figure 12(a). Another difference is the analysis procedure for H/W=0.63 wall is implicit static rather than implicit dynamic, because the author obtained a better failure pattern for the masonry from implicit static procedure.

Figure 12(a) shows the relationship between yield stress and plastic strain for expanded bricks under uniaxial compressive load modelled with Drucker-Prager material model. The expanded brick can bear nearly 16MPa peak uniaxial compression with a linear softening response. The air bag pressure - lateral displacement relationships for the FE model and the experiment specimen are compared in Figure 12(b), which shows the pressure increased gradually and then kept a constant value with the increase of lateral displacement. Initially, the pressure was resisted by the wall until it reached the maximum two-way bending capacity where diagonal cracks, then the horizontal cracks happened means only vertical bending capacity resist the pressure.

Maximum principle stress contour and cracking patterns are shown in Figure 13(a) and Figure 13(b) respectively. The cracking pattern includes four diagonal cracks caused by two-way bending moment and two horizontal cracks caused by vertical bending moment. It can be seen from Figure 13(a) that the distribution of maximum principle stress has highly consistence with the crack patterns, which means the tensile failure may happen not only in the joint, but also in the brick near the cracked joint.

4. Conclusion

In this paper, a mix-mode damage interaction constitutive model is applied in both detailed micro-modelling strategy for in-plane masonry walls and simplified micro-modelling strategy for out-of-plane masonry walls. Concrete damage plasticity material model and Drucker-Prager material model are used to simulate the nonlinear behaviour of expended bricks in different geometry walls under out-of-plane pressure.

The proposed interfacial modelling approach can avoid convergence difficulty with the help of the viscosity coefficient, which also improves the computing efficiency by the acceptable cost of accuracy. Compared with existing finite element models, the proposed model presented in this paper has the ability to predict the post-failure behaviour of masonry wall under different loading conditions exactly. Besides, the failure patterns of finite element wall models have quite well agreement with experimental results.

However, the complex mechanism of interface shear behaviour is still needed to be investigated. The combination of normal pressure and shear movement will result in frictional force that plays a critical role in the post failure behaviour in the shear direction. Another flaw of the proposed models is that neither the shear capacity nor the shear fracture energy is sensitive to the normal stress in the contact faces. According to Pluijm's (1992) study both shear strength and shear fracture energy have a positive linear relation with normal stress. Therefore, the authors will focus on a more functional interaction constitutive model in the future study.

Acknowledgement

The authors gratefully acknowledge the financial support of the Australian Research Council (through grants DP160102070 and DP190100797) and the Bushfire and Natural Hazards CRC for the work presented in this paper. The conclusion and opinions expressed herein are those of the authors and not necessarily of the sponsors.

Reference

Abdulla, K. F., Cunningham, L. S., & Gillie, M. (2017) Simulating masonry wall behaviour using a simplified micro-model approach. Engineering Structures, Vol 151, pp 349-365.

Andreotti, G., Graziotti, F., & Magenes, G. (2018) Detailed micro-modelling of the direct shear tests of brick masonry specimens: the role of dilatancy. Engineering Structures, Vol 168, pp 929-949.

Anthoine, A. (1995) Derivation of the in-plane elastic characteristics of masonry through homogenization theory. International journal of solids and structures, Vol 32, No 2, pp 137-163.

Benzeggagh, M. L., & Kenane, M. J. C. S. (1996) Measurement of mixed-mode delamination fracture toughness of unidirectional glass/epoxy composites with mixed-mode bending apparatus. Composites science and technology, Vol 56, No 4, pp 439-449.

Camanho, P. P., & Dávila, C. G. (2002) Mixed-mode decohesion finite elements for the simulation of delamination in composite materials. NASA/TM-2002-211737. VA, USA: NASA Langley Research Centre.

D'Altri, A. M., de Miranda, S., Castellazzi, G., & Sarhosis, V. (2018) A 3D detailed micro-model for the in-plane and out-of-plane numerical analysis of masonry panels. Computers & Structures, Vol 206, pp 18-30.

Gautam, D., Rodrigues, H., Bhetwal, K. K., Neupane, P., & Sanada, Y. (2016) Common structural and construction deficiencies of Nepalese buildings. Innovative Infrastructure Solutions, Vol 1, pp 1.

Kaushik, H. B., Rai, D. C., & Jain, S. K. (2007) Stress-strain characteristics of clay brick masonry under uniaxial compression. Journal of materials in Civil Engineering, Vol 19, No 9, pp 728-739.

Lee, J., & Fenves, G. L. (1998) Plastic-damage model for cyclic loading of concrete structures. Journal of engineering mechanics, Vol 124, No 8, pp 892-900.

Lotfi, H. R., & Shing, P. B. (1991) An appraisal of smeared crack models for masonry shear wall analysis. Computers & structures, Vol 41, No 3, pp 413-425.
Lotfi, H. R., & Shing, P. B. (1994) Interface model applied to fracture of masonry structures. Journal of structural engineering, Vol 120, pp 63-80.

Lourenço, P. B., & Rots, J. G. (1997) Multisurface interface model for analysis of masonry structures. Journal of engineering mechanics, Vol 123, pp 660-668.

Lourenço, P. J. B. B. (1997). Computational strategies for masonry structures. TU Delft: Delft University of Technology.

Hibbitt, H. D., Karlsson, B. I., & Sorensen, E. P. (2013) ABAQUS User's & Theory Manuals, 6.14. Dassault Systèmes Simulia Corp., Providence, RI, USA.

Ng, C. L. (1996) Experimental and theoretical investigation of the behaviour of brickwork cladding panel subjected to lateral loading. The University of Edinburgh.

Van der Pluijm, R. (1992) Material properties of masonry and its components under tension and shear. Proceedings 6th Canadian Masonry Symposium, 15-17 June 1992, Saskatoon, Canada, pp 675-686.

Vermeltfoort, A.Th. and Raijmakers, T.M.J. (1993) Deformation controlled meso shear tests on masonry piers, Part 2, Draft report, TU Eindhoven, The Netherlands (in Dutch)